Synchronization in networks with heterogeneous coupling delays

Andreas Otto* and Günter Radons†
Institute of Physics, Chemnitz University of Technology, 09107 Chemnitz, Germany

Dániel Bachrathy‡
Department of Applied Mechanics, Budapest University of Technology and Economics, H-1111, Budapest, Hungary

Gábor Orosz§
Department of Mechanical Engineering, University of Michigan, Ann Arbor, MI 48109, USA
(Dated: October 13, 2017)

Synchronization in networks of identical oscillators with heterogeneous coupling delays is studied. A decomposition of the network dynamics is obtained by diagonalizing a newly introduced adjacency lag operator which contains the topology of the network as well as the corresponding coupling delays. This generalizes the master stability function approach, which was developed for homogenous delays. As a result the network dynamics can be analyzed by delay differential equations with distributed delay, where different delay distributions emerge for different network modes. Frequency domain methods are used for the stability analysis of synchronized equilibria and synchronized periodic orbits. As an example, the synchronization behavior in a system of delay-coupled Hodgkin-Huxley neurons is investigated. It is shown that for increasing delay heterogeneity the parameter regions expand, where synchronized periodic spiking is unstable or even no synchronized periodic solution exists.

I. INTRODUCTION

Complex networks and synchronization phenomena are relevant in many fields. Specific examples can be found in social systems [1, 2], engineering [3–6], biology [7–10] and physics [11–13]. Some universal results on synchronization in complex networks have been summarized in [14, 15]. Often the interactions between nodes in the network are assumed to be instantaneous, which means that the state of one node immediately affects the state of other nodes. However, in many cases the signal propagation time between nodes is of the order of the internal time scales of the system. In such cases, time delays must be incorporated when modeling the connections between the network nodes. Some basic results on the dynamics of networks with time delayed couplings can be found in [16–18]. In some applications, like semiconductor lasers [11–13], the coupling delays can be tuned to be homogeneous. However, in general, the coupling delays are heterogeneous, i.e., there exist different delays for different connections in the network [5]. Such heterogeneity may affect the stability of synchronized equilibria and synchronized periodic orbits and lead to "amplitude death" in complex networks [19, 20].

Numerical simulations or statistical methods are often used to study the synchronization behavior in networks with heterogeneous delays [20–22]. However, a better understanding of the dynamics can be gained by analyzing the linear stability of specific solutions (equilibria, periodic orbits, heteroclinic orbits, chaotic motion). In particular, decomposing the dynamics into network modes in the vicinity of a particular solution allows systematic investigations of stability and bifurcations. The so-called master stability function approach combines such modal decomposition with linear stability analysis. This was first proposed for the analysis of complete synchronized solutions in networks with instantaneous couplings [23, 24] where stability properties were linked to the eigenvalues of the adjacency matrix. Similar decomposition were performed for nonidentical node dynamics [25, 26] and around cluster states [27–29].

Modal decomposition can be extended to networks with delay couplings [17]. This is possible even for multiple delays [30–32], and distributed delays in the connections [33]. However, in all these cases the delays were considered to be homogeneous, that is, the same delay distribution was used for all connections. An extension to heterogeneous delays was given in [34] with the restriction that the adjacency matrices corresponding to different coupling delays must commute. Another approach based on a timescale separation was presented for hierarchical networks having a small coupling delay within subnetworks and a large coupling delay between subnetworks [35]. A general approach for the modal decomposition around synchronized equilibria with heterogeneous coupling delays was introduced in [5]. Extending this method to synchronized time dependent solutions is not straightforward and we target this challenging problem in this paper.

We show that the stability of network modes in the vicinity of complete synchronized time dependent solutions can be analyzed by non-autonomous delay differential equations (DDEs) with distributed delays. The advantage of the present method is that, similar to the

* otto.a@mail.de
† radons@physik.tu-chemnitz.de
‡ bachrathy@mm.bme.hu
§ orosz@umich.edu

known master stability approach for networks with homogeneous delay, the dimension of this DDE system is equivalent to the dimension of the system that describes the dynamics at one network node. We show that for heterogeneous delay coupling the delay distribution of the DDE may change for different network modes, which differs from the classical master stability approach, where only a complex number (the eigenvalue of the adjacency matrix) may change for different network modes.

For synchronized periodic solutions we use a frequency domain approach for the stability analysis of the non-autonomous DDE with distributed delay. This method has been successfully applied to analyze the stability in machine tool vibrations [36, 37]. In the context of complex networks, synchronous oscillations of neurons are of special importance [7–10, 14]. Some results for synchronized solutions of networks of Hodgkin-Huxley neurons with homogeneous coupling delays were presented in [8, 10]. We apply the developed decomposition method to study the effects of heterogeneous coupling delays on such neural dynamics.

The paper is organized as follows. In Sec. II conditions for the existence of synchronized solutions in heterogeneous delay-coupled networks are given. In Sec. III the decomposition of the dynamics around time dependent solutions is performed. This is combined with numerical continuation in Sec. IV in order to study the stability and bifurcations of synchronized periodic orbits in a network of Hodgkin-Huxley neurons. We conclude our results in Sec. V.

II. SYNCHRONIZATION IN NETWORKS WITH HETEROGENEOUS DELAYS

A network of N identical oscillators with heterogeneous delay coupling is considered. In particular, R different coupling delays τ_r are considered. The dynamics of the configuration $\boldsymbol{x}_i \in \mathbb{R}^n$ of node i is modeled by the nonlinear DDE

$$\dot{\boldsymbol{x}}_i(t) = \boldsymbol{f}\big(\boldsymbol{x}_i(t)\big) + \sum_{r=1}^{R}\sum_{j=1}^{N} a_{r,ij}\, \boldsymbol{g}\big(\boldsymbol{x}_i(t), \boldsymbol{x}_j(t-\tau_r)\big). \quad (1)$$

The dynamics of the uncoupled node is described by the n dimensional nonlinear ordinary differential equation (ODE) $\dot{\boldsymbol{x}}_i = \boldsymbol{f}(\boldsymbol{x}_i)$, while the coupling function $\boldsymbol{g}(\boldsymbol{x}_i, \boldsymbol{x}_j)$ specifies how oscillator j influences the dynamics of oscillator i. The coefficients $a_{r,ij}$ are the elements of the N dimensional coupling matrices $\mathbf{A}_r$ corresponding to the delay τ_r specifying how strong the current configuration $\boldsymbol{x}_i(t)$ of node i is affected by the retarded configuration $\boldsymbol{x}_j(t-\tau_r)$ of node j with time delay τ_r. If $a_{r,ij} = 0$ there is no incoming signal at node i from node j with time delay τ_r. However, there can be an incoming connection between the same nodes with another delay. Moreover, the matrices $\mathbf{A}_r$ are not necessarily symmetric meaning that there can be an incoming connection but no outgoing connection with delay τ_r between the same nodes and vice versa. The sum $\sum_{r=1}^{R} \mathbf{A}_r = \mathbf{A}$ is also known as adjacency matrix and characterizes the complete topology of the network via a weighted directed graph, where the oscillators and the connections between them are the nodes and edges of the graph, respectively. Note that with $R \to \infty$, where the first sum in Eq. (1) becomes an integral, it is possible to take into account continuous distributions for the coupling delays.

A. Synchronization

In this paper completely synchronized solutions $\boldsymbol{x}_i(t) = \boldsymbol{x}_\mathrm{s}(t)$, $i = 1, \ldots, N$ of Eq. (1) are studied. These solutions are contained in the so-called synchronization manifold. The dynamics within this manifold is described by the DDE

$$\dot{\boldsymbol{x}}_s(t) = \boldsymbol{f}\big(\boldsymbol{x}_\mathrm{s}(t)\big) + \sum_{r=1}^{R} M_r\, \boldsymbol{g}\big(\boldsymbol{x}_\mathrm{s}(t), \boldsymbol{x}_\mathrm{s}(t-\tau_r)\big), \quad (2)$$

where M_r denotes the constant row sum of the separate coupling matrices $\mathbf{A}_r$, i.e.

$$M_{r,i} := \sum_{j=1}^{N} a_{r,ij} = M_r, \quad \text{for } i = 1, \ldots, N. \quad (3)$$

If for any coupling matrix $\mathbf{A}_r$ the row sum is not independent of the row index i, i.e. $\exists\, m, n \in [1, N]$ with $M_{r,m} \neq M_{r,n}$, it is not possible to define the synchronization manifold Eq. (2) meaning that, in general, only synchronized equilibria are possible [38]. In networks without coupling delays ($R = 1, \tau_1 = 0$) [23, 24] and in networks with homogeneous delays [17, 28] ($R = 1, \tau_1 \neq 0$) Eq. (3) is known as constant row sum condition. In networks with heterogeneous delays the constant row sum condition Eq. (3) must be fulfilled for each $r = 1, \ldots, R$. Note that for continuously distributed coupling delays, $R \to \infty$, the condition Eq. (3) for the existence of a synchronization manifold Eq. (2) means that there must be the same delay distribution M_r at each node of the network for all incoming connections.

To analyze the stability of synchronized solutions $\boldsymbol{x}_\mathrm{s}(t)$ we define the perturbations $\boldsymbol{y}_i(t) = \boldsymbol{x}_i(t) - \boldsymbol{x}_\mathrm{s}(t)$ whose dynamics can be approximated by the linear variational system

$$\dot{\boldsymbol{y}}_i(t) = \mathbf{L}(t)\, \boldsymbol{y}_i(t) + \sum_{r=1}^{R}\sum_{j=1}^{N} a_{r,ij}\, \mathbf{R}(t, \tau_r)\, \boldsymbol{y}_j(t-\tau_r), \quad (4)$$

where the coefficient matrices are defined as

$$\begin{aligned} \mathbf{L}(t) &= \mathrm{D}\boldsymbol{f}\big(\boldsymbol{x}_\mathrm{s}(t)\big) + \sum_{r=1}^{R} M_r\, \mathrm{D}_1\boldsymbol{g}\big(\boldsymbol{x}_\mathrm{s}(t), \boldsymbol{x}_\mathrm{s}(t-\tau_r)\big), \\ \mathbf{R}(t,\tau) &= \mathrm{D}_2\boldsymbol{g}\big(\boldsymbol{x}_\mathrm{s}(t), \boldsymbol{x}_\mathrm{s}(t-\tau)\big). \end{aligned} \quad (5)$$

The matrix $\mathrm{D}\boldsymbol{f}$ is the Jacobian of $\boldsymbol{f}$, and the matrices $\mathrm{D}_1\boldsymbol{g}$ and $\mathrm{D}_2\boldsymbol{g}$ are the derivatives of $\boldsymbol{g}$ with respect to the first and the second argument, respectively. Defining the nN dimensional column vector $\boldsymbol{y} = \mathrm{col}\,[\boldsymbol{y}_1, \ldots, \boldsymbol{y}_N]$ Eq. (4) can be rewritten as

$$\dot{\boldsymbol{y}}(t) = \big(\mathbf{I}_N \otimes \mathbf{L}(t)\big)\boldsymbol{y}(t) + \sum_{r=1}^{R} \big(\mathbf{A}_r \otimes \mathbf{R}(t,\tau_r)\big)\boldsymbol{y}(t-\tau_r), \quad (6)$$

where $\otimes$ denotes the Kronecker product and $\mathbf{I}_N$ denotes the $N \times N$ dimensional identity matrix. At this point, an important difference between networks with homogeneous delays and networks with heterogeneous delays appears. For heterogeneous delays both the matrices $\mathbf{A}_r$ and $\mathbf{R}(t,\tau_r)$ depend on the specific coupling delay τ_r. In other words, despite the same coupling function $\boldsymbol{g}$ appearing in all connections and for all delays τ_r, the coefficient matrices $\mathbf{R}(t,\tau_r)$ in the linearized dynamics Eq. (4) depends on the coupling delays τ_r through $\boldsymbol{x}_\mathrm{s}(t-\tau_r)$. This has consequences for the decomposition of the network dynamics, which is presented in Sec. III.

B. Tangential vs. transversal dynamics

The perturbation vector $\boldsymbol{y}$ in Eq. (6) can be divided into tangential perturbations and transversal perturbations [23, 24, 28]. If only tangential perturbations exist, each node undergoes the same perturbation $\boldsymbol{y}_i(t) = \boldsymbol{q}_1(t)$ for $i = 1, \ldots, N$, that is, $\boldsymbol{y}(t) = \mathrm{col}[\boldsymbol{q}_1(t), \ldots, \boldsymbol{q}_1(t)]$. Substituting this into (4) one obtains the dynamics for perturbations within the synchronization manifold

$$\dot{\boldsymbol{q}}_1(t) = \mathbf{L}(t)\boldsymbol{q}_1(t) + \sum_{r=1}^{R} M_r\, \mathbf{R}(t,\tau_r)\, \boldsymbol{q}_1(t-\tau_r), \quad (7)$$

that is indeed the linearization of Eq. (2). The transversal perturbations are defined as $\boldsymbol{y}_i(t) \neq \boldsymbol{y}_j(t)$ for at least one $i \neq j$.

Indeed, many different solutions may exist within the infinite dimensional synchronization manifold (equilibria, periodic orbits, homoclinic and heteroclinic orbits, chaos). Whereas tangential perturbations let the system stay within the synchronization manifold, transversal perturbations drive the system away from the synchronization manifold. Synchronization occurs only if the synchronized solution is transversally stable. The linearized dynamics of the network and its decomposition are discussed in detail in Sec. III.

C. Synchronized equilibria without synchronization manifold

Time delays can change the stability of an equilibrium but do not change the existence and location of the equilibrium [39, 40]. According to Eq. (1) synchronized equilibria of the network are defined by [38]

$$\boldsymbol{f}\big(\boldsymbol{x}_\mathrm{s}^*\big) + M\,\boldsymbol{g}\big(\boldsymbol{x}_\mathrm{s}^*, \boldsymbol{x}_\mathrm{s}^*\big) = 0, \quad (8)$$

where M denotes the constant row sum of the adjacency matrix $\mathbf{A}$, i.e.

$$M_i := \sum_{r=1}^{R}\sum_{j=1}^{N} a_{r,ij} = M, \quad \text{for } i = 1, \ldots, N. \quad (9)$$

Thus, as long as Eq. (9) holds, changing the delays of the connections does not change the existence of synchronized equilibria defined by Eq. (8). On the other hand, according to Eq. (3) changing the delays can change the existence of time dependent synchronized solutions. In other words, synchronized equilibria exist if the constant row sum condition is fulfilled for the adjacency matrix $\mathbf{A}$ but time dependent synchronized solution exist only if the constant row sum condition is fulfilled for all matrices $\mathbf{A}_r$ with $r = 1, \ldots, R$. Similarly, this means that time dependent synchronized states may exist for homogeneous delays (when Eq. (9) holds) but may be destroyed when adding heterogeneity to the delays (when Eq. (3) is not satisfied). In addition, according to Eq. (8) for $\boldsymbol{g}\big(\boldsymbol{x}_\mathrm{s}^*, \boldsymbol{x}_\mathrm{s}^*\big) = 0$ synchronized equilibria may exist even if Eq. (9) does not hold.

As a consequence, there is a large set of networks with heterogeneous delays, where synchronized equilibria $\boldsymbol{x}_\mathrm{s}^*$ exist but no time dependent synchronized solutions $\boldsymbol{x}_\mathrm{s}(t)$ are possible. In these cases, no synchronization manifold Eq. (2) can be defined and no tangential network mode exists. Indeed, if all transversal perturbations around the equilibrium decay the synchronized equilibrium is stable but when the equilibrium becomes unstable, an asynchronous state appears. In these networks stable synchronized equilibria occur due of identical node dynamics and identical coupling functions which is often referred to as amplitude death in the literature [41–43]. An overview on the different scenarios including the possibility for synchronized equilibria without a synchronization manifold is presented in Fig. 1.

III. DECOMPOSITION OF NETWORKS WITH HETEROGENEOUS COUPLING DELAYS

For characterizing the network dynamics with respect to complete synchronized solutions the analysis of Eq. (6) is necessary. However, from the analysis of Eq. (6) it is not clear if instabilities are related to tangential or transversal perturbations and the dimension of Eq. (6) can be very large. Therefore, more insight into the network dynamics can be gained by decomposing Eq. (6) into smaller subsystems. For networks without delay or with homogeneous delay we have $R = 1$ and the decomposition can be done, for example, by the eigenmode decomposition of the adjacency matrix $\mathbf{A} = \mathbf{A}_1$ [17, 23, 24, 28]. For networks with heterogeneous delays

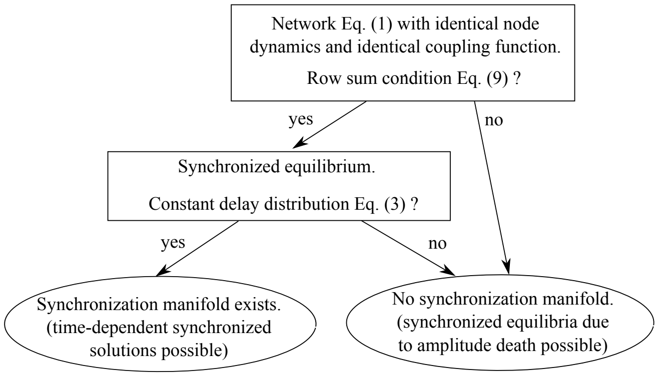

FIG. 1. Complete synchronization and amplitude death in networks with heterogeneous delays.

the same decomposition is still possible if all matrices $\mathbf{A}_r$, $r = 1, \dots, R$ commute with each other [34]. However, in most cases the matrices $\mathbf{A}_r$ do not commute. For the analysis of synchronized equilibria a general approach for the decomposition was introduced in [5]. The idea is the eigenmode decomposition of the matrix

$$\hat{\mathbf{B}}(s) = \sum_{r=1}^{R} \mathbf{A}_r \, \mathrm{e}^{-s\tau_r}, \tag{10}$$

which can be derived from the Laplace domain representation of Eq. (6) (s is the Laplace variable) and combines the information on the coupling topology and the coupling delays.

However, we will show in the following that an eigenvalue decomposition of the matrix $\hat{\mathbf{B}}(s)$ as proposed in [5] is, in general, not suitable for the decomposition of the network dynamics around time dependent solutions. The reason is that, in general, the left and the right eigenvectors of the matrix $\hat{\mathbf{B}}(s)$ depend on s and are therefore not invariant. Indeed, for synchronized equilibria with time-invariant coefficient matrices $\mathbf{L}(t) = \mathbf{L}_0$ and $\mathbf{R}(t,\tau) = \mathbf{R}_0$ a diagonalization of the matrix $\hat{\mathbf{B}}(s)$ is very helpful because it decomposes Eq. (6) into a system of N uncoupled subsystems of dimension n, where each n dimensional subsystem determines the dynamics of one network eigenmode. However, we will show that for the time dependent case the diagonalization of the matrix $\hat{\mathbf{B}}(s)$ does not necessarily decompose the network dynamics into uncoupled subsystems. Thus, in this paper we are searching for a decomposition of the matrix $\hat{\mathbf{B}}(s)$ with invariant left or right subspaces, which decomposes the network dynamics into smaller subsystems even in the time dependent case.

In the next subsection we first explain what we mean with a network decomposition since there are different levels for decomposing the dynamics of a complex networks with time delays. Thereafter, in Sec. III B we introduce a representation of the network dynamics in terms of lag operators because we show our approach in the time domain. This is complementary to [5] and we think that it is more illustrative in case of time dependent synchronized solutions. In Sec. III C the decomposition of the network with heterogeneous delays around time dependent solutions is presented followed by some examples in Sec. III D.

A. Three decomposition levels

Delay-coupled networks are infinite dimensional systems due to the existence of time delays τ_r in the coupling terms, i.e., the initial condition for Eq. (4) are functions on the interval $[-\tau_{\max}, 0]$ for the vector $\boldsymbol{y} \in \mathbb{R}^{nN}$, where $\tau_{\max}$ is the maximum delay. This means that the state at time t can be defined by the function $\boldsymbol{y}(t+\theta)$, $-\tau_{\max} \le \theta \le 0$ [44, 45]. Roughly speaking the network is $N \times n \times \infty$ dimensional.

Three different levels of decomposition of delay-coupled networks may be identified. The first level is the network level, which focuses on the N nodes coupled via the edges of the graph. A decomposition at the network level decomposes the dynamics into N network modes. If Eq. (3) is fulfilled, one tangential and $N-1$ transversal network modes exist [10, 17, 23, 24]. The second level is the node level corresponding to the n scalar equations specifying the dynamics at each node that may be decomposed into n scalar DDEs; see [46, 47] where the scalar Lambert W function was utilized. For example, one may decompose Eq. (7) for the tangential dynamics into n scalar DDEs. The third level is the delay level. In particular, a scalar DDE can be further decomposed into infinitely many ODEs corresponding to the characteristic roots [44, 48, 49]. The node level and the delay level are often handled together using Operator Differential Equations [44] or Matrix Lambert W function [50].

In the remaining part of this paper we focus on the decomposition at the network level. Indeed, such a decomposition is not always possible. For example, networks with non-identical node dynamics, i.e., using $\boldsymbol{f}_i$ instead of $\boldsymbol{f}$ in Eq. (1) yield $\mathbf{L}_i$ instead of $\mathbf{L}$ in Eq. (4). In this case, the Kronecker product in Eq. (6) cannot be constructed and a decomposition at the network level is not possible in general. A decomposition combining the network and the node level is still possible but in such a case the corresponding modes are less descriptive.

B. Representation with lag operators

We are searching for a time domain representation of the network dynamics in terms of an operator that contains the information on the network topology and the coupling delays similar to the matrix $\hat{\mathbf{B}}(s)$ defined in Eq. (10). Thus, we introduce the lag operator $\mathcal{S}(\tau)$ defined by

$$\mathcal{S}(\tau)\, y(t) = y(t-\tau), \tag{11}$$

for a scalar-valued function $y(t)$. Indeed, this can be extended to vector valued functions. An alternative representation of the lag operator can be derived from the Taylor expansion of $y(t-\tau)$ about $\tau = 0$ and is given by $\mathcal{S}(\tau) = \mathrm{e}^{-\tau \frac{d}{dt}}$. The eigenfunctions of the lag operator are exponential functions independent of the time lag, that is,

$$\mathcal{S}(\tau)\,\mathrm{e}^{st} = \mathrm{e}^{-s\tau}\,\mathrm{e}^{st}\,. \tag{12}$$

As a consequence, lag operators with different arguments commute with each other and fulfill the relation

$$\mathcal{S}(\tau_1)\mathcal{S}(\tau_2) = \mathcal{S}(\tau_2)\mathcal{S}(\tau_1) = \mathcal{S}(\tau_1 + \tau_2). \tag{13}$$

It follows that $\mathcal{S}^n(\tau) = \mathcal{S}(n\tau)$ and the identity element is denoted by $\mathcal{S}(0)$. Obviously, the lag operator commutes also with the differential operator $\frac{d}{dt}\mathcal{S}(\tau) = \mathcal{S}(\tau)\frac{d}{dt}$.

With the introduction of the lag operator, the linearized dynamics Eq. (6) can be written as

$$\dot{\boldsymbol{y}}(t) = \Big(\mathbf{I}_N \otimes \mathbf{L}(t) + \sum_{r=1}^{R} \mathbf{A}_r \mathcal{S}(\tau_r) \otimes \mathbf{R}(t,\tau_r)\Big)\boldsymbol{y}(t). \tag{14}$$

We remark that when calculating the elements of the Kronecker product $\mathbf{A}_r\mathcal{S}(\tau_r) \otimes \mathbf{R}(t,\tau_r)$ the lag operators do not act on $\mathbf{R}(t,\tau_r)$; see (6). Since the matrix $\mathbf{R}(t,\tau_r)$ may change its shape in each term of the sum in Eq. (14), in general, a decomposition at the network level is not possible. In this paper we focus on a delay-independent coefficient matrix $\mathbf{R}(t,\tau) = \mathbf{R}(t)$ for the coupling term. There are two cases, where $\mathbf{R}(t,\tau)$ does not dependent on τ. The first case is the case of synchronized equilibria $\boldsymbol{x}_\mathrm{s}(t) = \boldsymbol{x}_\mathrm{s}(t-\tau) \equiv \boldsymbol{x}_\mathrm{s}^*$, which results in constant matrices $\mathbf{R} = \mathbf{D}_2\boldsymbol{g}(\boldsymbol{x}_\mathrm{s}^*, \boldsymbol{x}_\mathrm{s}^*)$. The second case is when the coupling is of the form $\boldsymbol{g}(\boldsymbol{x}_i(t), \boldsymbol{x}_j(t-\tau_r)) = \mathbf{G}(\boldsymbol{x}_i(t)) \cdot \boldsymbol{x}_j(t-\tau_r)$, which yields $\mathbf{R}(t) = \mathbf{G}(\boldsymbol{x}_\mathrm{s}(t))$. In these cases Eq. (14) can be simplified to

$$\dot{\boldsymbol{y}}(t) = (\mathbf{I}_N \otimes \mathbf{L}(t) + \mathcal{B} \otimes \mathbf{R}(t))\,\boldsymbol{y}(t), \tag{15}$$

where the so-called adjacency lag operator $\mathcal{B}$ is defined by

$$\mathcal{B} = \sum_{r=1}^{R} \mathbf{A}_r \mathcal{S}(\tau_r). \tag{16}$$

Similar to the corresponding Laplace domain representation $\hat{\mathbf{B}}(s)$ shown earlier in Eq. (10), the adjacency lag operator contains all information on the network topology (given by the matrices $\mathbf{A}_r$) and the coupling delays (specified by the lag operators $\mathcal{S}(\tau_r)$).

C. Decomposition of the adjacency lag operator

The adjacency lag operator $\mathcal{B}$ contains the lag operators $\mathcal{S}(\tau_r)$ defined in Sec. III B. Due to the commutative property (13) these operators can be handled like commuting symbols. At first we will show why a formal diagonalization of the operator $\mathcal{B}$ or the matrix $\hat{\mathbf{B}}(s)$, respectively, as presented in [5] does not necessarily decouple the linearized dynamics around time dependent synchronized solutions. Later, we show an alternative approach for the decomposition to overcome this problem.

Ideally, we are searching for a diagonalization of the adjacency lag operator $\mathcal{B}$ as

$$\begin{aligned} &\mathcal{B}\,\mathcal{V}_k = \mathcal{D}_k\,\mathcal{V}_k, \\ &\mathcal{U}_k\,\mathcal{B} = \mathcal{D}_k\,\mathcal{U}_k, \quad k = 1,\dots,N, \end{aligned} \tag{17}$$

where $\mathcal{D}_k$ is an operator-valued eigenvalue while $\mathcal{V}_\ell$ and $\mathcal{U}_k$ are the N dimensional operator-valued right and left eigenvectors in column and row format, respectively. These form a bi-orthogonal system with $\mathcal{U}_k \cdot \mathcal{V}_\ell = \delta_{k\ell}$, where $\delta_{k\ell}$ denotes the Kronecker delta. In general, $\mathcal{D}_k$, $\mathcal{V}_k$, $\mathcal{U}_k$ can contain linear and nonlinear functions of the lag operators $\mathcal{S}(\tau_r)$. We assume that the diagonalization Eq. (17) exists, i.e. algebraic and geometric multiplicity are the same for each eigenvalue $\mathcal{D}_k$ of $\mathcal{B}$. Using the operator-valued eigenvectors $\mathcal{V}_k$ and $\mathcal{U}_k$ we define the new variables

$$\boldsymbol{q}_k(t) = (\mathcal{U}_k \otimes \mathbf{I}_n)\,\boldsymbol{y}(t), \tag{18}$$

and use them to construct the solution as

$$\boldsymbol{y}(t) = \sum_{\ell=1}^{N} (\mathcal{V}_\ell \otimes \mathbf{I}_n)\,\boldsymbol{q}_\ell(t). \tag{19}$$

Then the dynamics in the new basis can be obtained by multiplying Eq. (15) with $\mathcal{U}_k \otimes \mathbf{I}_n$ from the left, substituting Eq. (19) and using Eq. (17) and Eq. (18). This yields

$$\dot{\boldsymbol{q}}_k(t) = \sum_{\ell=1}^{N} \left(\mathcal{U}_k\,[\mathbf{L}(t)]\,\mathcal{V}_\ell + \mathcal{U}_k\,[\mathbf{R}(t)]\,\mathcal{V}_\ell\mathcal{D}_\ell\right)\boldsymbol{q}_\ell(t), \tag{20}$$

where we have used the abbreviated notation $\mathcal{U}_k\,[\mathbf{L}(t)]\,\mathcal{V}_\ell = (\mathcal{U}_k \otimes \mathbf{L}(t))(\mathcal{V}_\ell \otimes \mathbf{I}_n)$, i.e., the lag operators in $\mathcal{U}_k$ act on $\mathbf{L}(t)$, whereas $\mathcal{V}_\ell$ does not act on $\mathbf{L}(t)$. If the coefficient matrices $\mathbf{L}(t) = \mathbf{L}_0$ and $\mathbf{R}(t) = \mathbf{R}_0$ are time invariant (which happens around synchronized equilibria [5]), $\mathcal{U}_k\,[\mathbf{L}_0]\,\mathcal{V}_\ell = \mathbf{L}_0\delta_{k\ell}$ and similar statement holds for the term with $\mathbf{R}_0$. As a consequence, Eq. (20) decouples into N independent n dimensional subsystems, where each $\boldsymbol{q}_k$ and $\mathcal{V}_k$ are the modal coordinates and the mode shapes of the network eigenmodes, respectively. In contrast, since $\mathcal{U}_k$ and $\mathcal{V}_k$ can contain lag operators, for time dependent coefficient matrices, in general, Eq. (20) is not decoupled because $\mathcal{U}_k\,[\mathbf{L}(t)]\,\mathcal{V}_\ell \neq \mathbf{L}(t)\delta_{k\ell}$. A paradigmatic example for such a coupling term can be given by $\mathcal{U}_k\,[\mathbf{L}(t)]\,\mathcal{V}_\ell = \mathbf{L}(t) - \mathbf{L}(t-\tau_r)$ for $k \neq l$. Thus, even if the adjacency lag operator $\mathcal{B}$ or equivalently the matrix $\hat{\mathbf{B}}(s)$ is diagonalized, for the time dependent case it is not necessarily true that the network dynamics Eq. (15) represented in the new basis Eq. (20) automatically decomposes into N subsystems describing the dynamics of N decoupled network eigenmodes.

Nevertheless, it is worth taking a closer view on Eq. (20). Often $\mathcal{V}_k$ and/or $\mathcal{U}_k$ contain no lag operators (but numbers only). This happens if the matrices $\mathbf{A}_r$ have simultaneous right or left eigenvectors, respectively. Then, the corresponding operators $\mathcal{D}_k$ are given by

$$\mathcal{D}_k = \sum_{r=1}^{R} \sigma_{r,k} \mathcal{S}_r, \tag{21}$$

where $\sigma_{r,k}$ are the corresponding eigenvalues of the matrix $\mathbf{A}_r$. For example, if the right eigenvectors contain only numbers, that is $\mathcal{V}_\ell = \mathbf{V}_\ell$, we have $\mathcal{U}_k\,[\mathbf{L}(t)]\,\mathbf{V}_\ell = \mathbf{L}(t)\delta_{k\ell}$. The same holds for the terms with $\mathbf{R}(t)$ and if the left eigenvectors contain only numbers, i.e. $\mathcal{U}_k = \mathbf{U}_k$. As a consequence, many of the coupling terms in Eq. (20) vanish. By considering all coordinates $\boldsymbol{q}_k(t)$, $k = 1, \ldots, N$ the structure of Eq. (20) can be illustrated as in Fig. 2(a). In particular, we distinguish between three different types of modes whose stability can be analyzed separately.

We first consider the modes $k = 1, \ldots, k_1$, where the left eigenvectors contain only numbers, i.e. $\mathcal{U}_k = \mathbf{U}_k$. This means that according to Eq. (20) the modal dynamics for $k = 1, \ldots, k_1$ are completely decoupled and can be described by

$$\dot{\boldsymbol{q}}_k(t) = (\mathbf{L}(t) + \mathbf{R}(t)\,\mathcal{D}_k)\,\boldsymbol{q}_k(t). \tag{22}$$

This corresponds to the upper row in Fig. 2 and the elements on the main diagonal are given by Eq. (22). We call these *master modes* because they can drive the remaining modes of the network. Note that since $\mathcal{D}_k\,\boldsymbol{q}_k(t) = \sum_{r=1}^{R} \sigma_{r,k}\,\boldsymbol{q}_k(t-\tau_r)$ (cf. Eq. (21)), Eq. (22) is a DDE with distributed delay $\sum_{r=1}^{R} \sigma_{k,r}\,\delta(\tau-\tau_r)$, where δ denotes the Dirac delta function.

Second, we consider the modes $k = k_2+1, \ldots, N$, where the $\mathcal{U}_k$ contain lag operators while the $\mathcal{V}_k$ contain only numbers as illustrated in the lowest row in Fig. 2. Since in this case $\mathcal{U}_k\,[\mathbf{L}(t)]\,\mathbf{V}_\ell = \mathbf{L}(t)\delta_{k\ell}$ for the terms in the sum of Eq. (20) with $\ell = k_2+1, \ldots, N$, the corresponding coupling terms vanish meaning that these modes do not drive any other mode. Consequently, the off-diagonal terms in the last column in Fig. 2(a) are zero. However, since the off-diagonal terms in the lower left corner with $k > k_2$ and $\ell \le k_2$ do not necessarily vanish these modes can be driven by other modes and we call them *slave modes*. Similarly to the master modes the main diagonal elements of the slave modes are described by Eq. (22).

The third type of modes with $k = k_1+1, \ldots, k_2$ are called *intermediate modes* shown in the middle row in Fig. 2(a). In this case $\mathcal{U}_k$ and $\mathcal{V}_k$ may contain lag operators and the dynamics within the intermediate modes is not decoupled illustrated by the large block in the middle of the matrix scheme in Fig. 2(a). In order to decouple the intermediate modes from each other, a modified decomposition of the adjacency lag operator $\mathcal{B}$ different from the eigenmode decomposition Eq. (17) is necessary.

More precisely, we are searching for a decomposition with an invariant left or right subspace. We can find such a transformation by a block diagonalization of the adjacency lag operator $\mathcal{B}$, where we obtain $Q \times Q$ dimensional blocks of lag operators $\mathcal{D}_{p,\ldots,q}$ for the intermediate modes with $Q = q-p+1 > 1$. In particular, for the intermediate modes $k = p, \ldots, q$ we use the decomposition

$$\begin{aligned} \mathcal{B}\,\mathcal{V}_{p,\ldots,q} &= \mathcal{D}_{p,\ldots,q}\,\mathcal{V}_{p,\ldots,q}, \\ \mathcal{U}_{p,\ldots,q}\,\mathcal{B} &= \mathcal{D}_{p,\ldots,q}\,\mathcal{U}_{p,\ldots,q}, \end{aligned} \tag{23}$$

where $\mathcal{V}_{p,\ldots,q}$ and $\mathcal{U}_{p,\ldots,q}$ represent blocks of size $N \times Q$ and $Q \times N$, respectively, and $\mathcal{U}_{p,\ldots,q} \cdot \mathcal{V}_{p,\ldots,q}$ results in the Q dimensional identity matrix. Specifically, we construct Eq. (23) in such a way that $\mathcal{U}_{p,\ldots,q}$ or $\mathcal{V}_{p,\ldots,q}$ contain only numbers, which makes use of common invariant right or left subspaces of the matrices $\mathbf{B}_r$ and implies that the elements of $\mathcal{D}_{p,\ldots,q}$ are given by linear combinations of the lag operators $\mathcal{S}(\tau_r)$. As a result the intermediate modes are further decomposed into intermediate master modes ($\mathcal{U}_{p,\ldots,q}$ containing only numbers) and intermediate slave modes ($\mathcal{V}_{p,\ldots,q}$ containing only numbers); cf. Fig. 2(b). In this case the $nQ \times nQ$ dimensional blocks on the main diagonal of the intermediate modes, illustrated by the small quadratic blocks in Fig. 2(b), can be described by

$$\dot{\boldsymbol{q}}_{p,\ldots,q}(t) = \left(\mathbf{I}_Q \otimes \mathbf{L}(t) + \frac{1}{N}\mathcal{D}_{p,\ldots,q} \otimes \mathbf{R}(t)\right) \boldsymbol{q}_{p,\ldots,q}(t), \tag{24}$$

where $\boldsymbol{q}_{p,\ldots,q}(t)$ is an nQ dimensional column vector. A concrete example for $\mathcal{D}_{p,\ldots,q}$ is given in Sec. III D.

From the detailed view on Eq. (20) we can conclude that, in contrast to the case of synchronized equilibria, for time dependent synchronized solutions a diagonalization of $\mathcal{B}$ does not decouple the network dynamics. Instead, a block triangular structure appears for the network dynamics; see Fig. 2a). If the modified decomposition Eq. (23) is used a further decomposition of the intermediate modes into smaller subblocks may be possible. Similar to the fact, that the eigenvalues of a triangular matrix are equal to the diagonal elements, the stability of the network can be analyzed by studying the blocks on the main diagonal of Eq. (20). These blocks are given by Eq. (22) for the master and the slave modes and are given by Eq. (24) for the intermediate modes. A frequency domain method for the accurate and efficient stability analysis of Eq. (22) and Eq. (24) is presented in Appendix A. If a slave mode becomes unstable only the corresponding $\boldsymbol{q}_k(t)$ grows exponentially. On the other hand, for an unstable master mode in addition the perturbations $\boldsymbol{q}_\ell(t)$ corresponding to all driven intermediate and slave modes grow exponentially. Finally, we remark that the tangential mode is always a slave mode because by definition we have $\mathcal{V}_1 = \mathbf{V}_1 = [\ 1, \ldots, 1\ ]^{\mathrm{T}}$ meaning

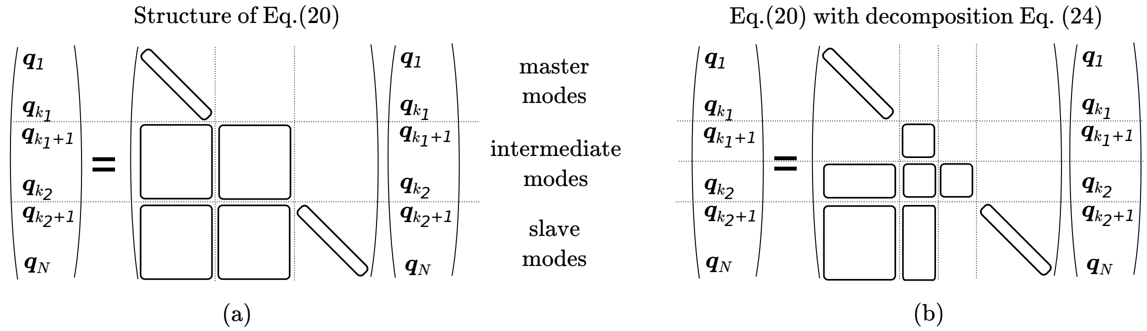

FIG. 2. (a) Structure of Eq. (20) with separation into master modes ($\mathcal{U}_k$ contains only numbers), slave modes ($\mathcal{V}_k$ contains only numbers) and intermediate modes. Only the squares and the diagonal stripes are non-empty. The stripes at the main diagonal are associated with Eq. (22) and determine the stability of the master and the slave modes, respectively. The intermediate modes are driven by the master modes and both can drive the slave modes. (b) Structure of Eq. (20) after additional decomposition of the intermediate modes. The two small squares at the main diagonal of the intermediate modes are associated with two blocks similar to Eq. (24), specifying the stability of the intermediate modes.

that the tangential eigenmode cannot drive transversal eigenmodes.

D. Examples

As an illustration, two examples with $N = 5$ nodes and two different coupling delays are studied. The first one is a special case of all-to-all coupling without self-coupling

$$\mathcal{B} = \begin{bmatrix} 0 & \mathcal{S}(\tau_1) & \mathcal{S}(\tau_1) & \mathcal{S}(\tau_1) & \mathcal{S}(\tau_2) \\ \mathcal{S}(\tau_1) & 0 & \mathcal{S}(\tau_2) & \mathcal{S}(\tau_1) & \mathcal{S}(\tau_1) \\ \mathcal{S}(\tau_1) & \mathcal{S}(\tau_2) & 0 & \mathcal{S}(\tau_1) & \mathcal{S}(\tau_1) \\ \mathcal{S}(\tau_1) & \mathcal{S}(\tau_1) & \mathcal{S}(\tau_1) & 0 & \mathcal{S}(\tau_2) \\ \mathcal{S}(\tau_2) & \mathcal{S}(\tau_1) & \mathcal{S}(\tau_1) & \mathcal{S}(\tau_1) & 0 \end{bmatrix}. \tag{25}$$

Notice that for this example the adjacency matrix $\mathbf{A}$ is symmetric but the adjacency lag operator $\mathcal{B}$ is not symmetric as $\mathcal{B}_{45} \neq \mathcal{B}_{54}$. The operator-valued eigenvalues after diagonalization of $\mathcal{B}$ as described in Eq. (17) are

$$\begin{aligned} \mathcal{D}_1 &= 3\mathcal{S}(\tau_1) + \mathcal{S}(\tau_2), \\ \mathcal{D}_2 &= -2\mathcal{S}(\tau_1) + \mathcal{S}(\tau_2), \\ \mathcal{D}_3 &= -\mathcal{S}(\tau_1), \\ \mathcal{D}_4 &= -\mathcal{S}_(\tau_2), \\ \mathcal{D}_5 &= -\mathcal{S}_(\tau_2). \end{aligned} \tag{26}$$

All $\mathcal{D}_k$, $k = 1, \ldots, N$ in Eq. (26) are a linear combination of lag operators as in Eq. (21). This means that only master and slave modes appear and Eq. (22) can be used for the stability analysis of all network eigenmodes. The corresponding operators $\mathcal{U}_k$ and $\mathcal{V}_k$ can be found in Appendix B. Notice the algebraic multiplicity $\mathcal{D}_4 = \mathcal{D}_5$ that also results in geometric multiplicity. This means that $\mathcal{V}_4$ and $\mathcal{V}_5$ (and similarly $\mathcal{U}_4$ and $\mathcal{U}_5$) are not unique but here they are constructed such that orthogonality is satisfied.

The second example is referred to as general coupling and is defined by the adjacency lag operator

$$\mathcal{B} = \begin{bmatrix} 0 & \mathcal{S}(\tau_1) & 0 & \mathcal{S}(\tau_1) & \mathcal{S}(\tau_2) \\ 0 & 0 & \mathcal{S}(\tau_2) & \mathcal{S}(\tau_1) & \mathcal{S}(\tau_1) \\ \mathcal{S}(\tau_1) & \mathcal{S}(\tau_2) & 0 & 0 & \mathcal{S}(\tau_1) \\ \mathcal{S}(\tau_1) & 0 & \mathcal{S}(\tau_1) & 0 & \mathcal{S}(\tau_2) \\ \mathcal{S}(\tau_2) & \mathcal{S}(\tau_1) & 0 & \mathcal{S}(\tau_1) & 0 \end{bmatrix}. \tag{27}$$

A diagonalization as described in Eq. (17) yields the operator-valued eigenvalues

$$\begin{aligned} \mathcal{D}_1 &= 2\mathcal{S}(\tau_1) + \mathcal{S}(\tau_2), \\ \mathcal{D}_2 &= -\mathcal{S}(\tau_1) + \mathcal{S}(\tau_2), \\ \mathcal{D}_3 &= -\mathcal{S}(\tau_2), \\ \mathcal{D}_4 &= \tfrac{1}{2}\Big(-\big(\mathcal{S}(\tau_1) + \mathcal{S}(\tau_2)\big) \\ &\qquad + \sqrt{\mathcal{S}^2(\tau_2) - 2\mathcal{S}(\tau_1)\mathcal{S}(\tau_2) - 3\mathcal{S}^2(\tau_1)}\Big), \\ \mathcal{D}_5 &= \tfrac{1}{2}\Big(-\big(\mathcal{S}(\tau_1) + \mathcal{S}(\tau_2)\big) \\ &\qquad - \sqrt{\mathcal{S}^2(\tau_2) - 2\mathcal{S}(\tau_1)\mathcal{S}(\tau_2) - 3\mathcal{S}^2(\tau_1)}\Big), \end{aligned} \tag{28}$$

where $\mathcal{D}_4$ and $\mathcal{D}_5$ correspond to intermediate modes. This means that for time dependent solutions the formal diagonalization of $\mathcal{B}$ does not necessarily lead to uncoupled network dynamics for the intermediate modes. As a consequence, Eq. (22) with $\mathcal{D}_4$ and $\mathcal{D}_5$ from Eq. (28) can be used only for the stability analysis around an equilibrium. In this case the nonlinear combinations of the lag operators appearing in $\mathcal{D}_4$ and $\mathcal{D}_5$ can be defined via multi-variable Taylor series [5]. For time dependent synchronized solutions a decomposition similar to Eq. (24) is necessary, where

$$\mathcal{D}_{4,5} = \begin{bmatrix} -\mathcal{S}(\tau_1) & \mathcal{S}(\tau_1) \\ -\mathcal{S}(\tau_1) & -\mathcal{S}(\tau_2) \end{bmatrix}. \tag{29}$$

The mode shapes $\mathcal{U}_{4,5}$ ($\mathcal{V}_{4,5}$) for the modified decomposition are given in Appendix B, where $\mathcal{U}_{4,5}$ ($\mathcal{V}_{4,5}$) are constructed as a linear combination of $\mathcal{U}_4$ and $\mathcal{U}_5$ ($\mathcal{V}_4$ and $\mathcal{V}_5$). Obviously, the formal diagonalization of $\mathcal{D}_{4,5}$ again lead to the operator-valued eigenvalues $\mathcal{D}_4$ and $\mathcal{D}_5$ as defined in Eq. (28) and this property can be also used to construct $\mathcal{D}_{4,5}$.

IV. DELAY-COUPLED HODGKIN-HUXLEY NEURONS

In this section we study the synchronized solutions in a network of N delay-coupled Hodgkin-Huxley neurons with heterogeneous delays [8, 10, 51]. In the following numerical analysis the modal decomposition from Sec. III is used, which means that we take the advantage of analyzing the modal dynamics Eq. (22) with different delay distributions instead of the full network dynamics. We use the frequency domain method from Appendix A for the stability analysis of the non-autonomous DDE with distributed delay. Apart from the lower dimension of Eq. (22) compared to the full network dynamics, the decomposed analysis gives us some additional information on the stability of the particular network modes.

The time evolution of the Hodgkin-Huxley neuronal network is given by the DDE

$$\begin{aligned} C\dot{V}_i(t) = I &- g_{\mathrm{Na}}\, m_i^3(t)\, h_i(t)\big(V_i(t) - V_{\mathrm{Na}}\big) \\ &- g_{\mathrm{K}}\, n_i^4(t)\,\big(V_i(t) - V_{\mathrm{K}}\big) \\ &- g_{\mathrm{L}}\,\big(V_i(t) - V_{\mathrm{L}}\big) \\ &+ \frac{\kappa}{N}\sum_{r=1}^{R} a_{r,ij}\big(V_j(t-\tau_r) - V_i(t)\big), \\ \dot{m}_i =& \alpha_m\big(V_i(t)\big)\big(1 - m_i(t)\big) - \beta_m\big(V_i(t)\big)m_i(t), \\ \dot{h}_i =& \alpha_h\big(V_i(t)\big)\big(1 - h_i(t)\big) - \beta_h\big(V_i(t)\big)h_i(t), \\ \dot{n}_i =& \alpha_n\big(V_i(t)\big)\big(1 - n_i(t)\big) - \beta_n\big(V_i(t)\big)n_i(t), \end{aligned} \tag{30}$$

for $i = 1, \ldots, N$. Here the time t is measured in ms. The symbol V_i denotes the voltage of the i-th neuron at the soma (measured in mV) while the dimensionless gating variables $m_i, h_i, n_i \in [0,1]$ characterize the "openness" of the ion channels embedded in the cell membrane. The specific form of the nonlinear functions $\alpha_m(V)$, $\alpha_h(V)$, $\alpha_n(V)$ and $\beta_m(V)$, $\beta_h(V)$, $\beta_n(V)$ are given in Eq. (C1), while the reference voltages V_{Na}, V_{K}, V_{L}, the conductances g_{Na}, g_{K}, g_{L}, the membrane capacitance C, the driving current I, and the number of neurons N are given in Table I in Appendix C. The last term in the voltage equation in Eq. (30) represents a direct electronic connection of conductance κ between the axon of the j-th neuron and the dendrites of the i-th neuron, that is, $V_i(t)$ represents the postsynaptic potential while $V_j(t-\tau_r)$ represents the presynaptic potential and the delay τ_r stands for the signal propagation time along the axon of the j-th neuron (dendritic delays are omitted here). That is, the presynaptic potential is equal to what the potential of the soma of the jth neuron was τ_r time before.

In order to represent the decomposition techniques established above the examples with all-to-all coupling Eq. (25) and the general coupling Eq. (27) are considered with the conductances fixed at $\kappa = 1.2\frac{\mathrm{mS}}{\mathrm{cm}^2}$ and $\kappa = 1.6\frac{\mathrm{mS}}{\mathrm{cm}^2}$, respectively. The different values of the coupling strengths compensate the different row sums of the two coupling schemes, i.e., κM is the same in the two examples. Consequently, the tangential dynamics Eq. (7) are equivalent in the two cases when considering homogeneous delays $\tau_1 = \tau_2$; see [10]. We vary the delays and study how the stability of the equilibria and periodic orbits change.

A. Synchronized equilibria

For the parameters considered here, Eq. (30) has a unique equilibrium; see [10]. Fig. 3(a) and (b) show the stability charts for the equilibrium in the (τ_1, τ_2)-plane for all-to-all coupling (Eq. (25)) and general coupling (Eq. (27)), respectively. The stable domains are shaded. When crossing the thick black curves starting from the shaded area, the dominant characteristic root corresponding to the tangential eigenmode crosses the imaginary axis and the synchronized equilibrium bifurcates to synchronized periodic solutions. Notice that along the diagonal $\tau_1 = \tau_2$ of homogeneous delays, tangential stability losses occur at the same locations in both panels. When crossing the thin curves, either by setting $\tau_1 \neq \tau_2$ or by making the coupling more general, characteristic roots corresponding to transversal eigenmodes cross the imaginary axis. If this happens while starting from the shaded regions, the synchronized equilibrium becomes unstable with respect to transversal perturbations and synchronization is broken. In this case typically cluster-synchronized periodic solutions appear [52].

In order to emphasize the effects of delay heterogeneity we show the real part λ of the dominant characteristic roots s for the case with general coupling in Fig. 4. In Fig. 4(a) and (b) we vary the delays along the identity $\tau_1 = \tau_2$ and along $\tau_2 = \tau_1 + 4.8$ ms, i.e., along the dotted and dashed line in Fig. 3(b), respectively. For the homogeneous case $\tau_1 = \tau_2$ both tangential and transversal stability losses occur and the synchronized equilibrium is stable only for $\tau_1 \in [1.7, 2.4]$ and $\tau_1 \in [3.9, 4.5]$. In contrast, for the heterogeneous case $\tau_2 = \tau_1 + 4.8$ ms tangential instabilities vanish and the stable regions are larger compared to the homogeneous case. Heterogeneous delays not always increase the stable regions. However, properly tuned delay distributions can be used to stabilize the system dynamics, as it is used, for example, in industrial applications for the suppression of machine tool chatter [53–55].

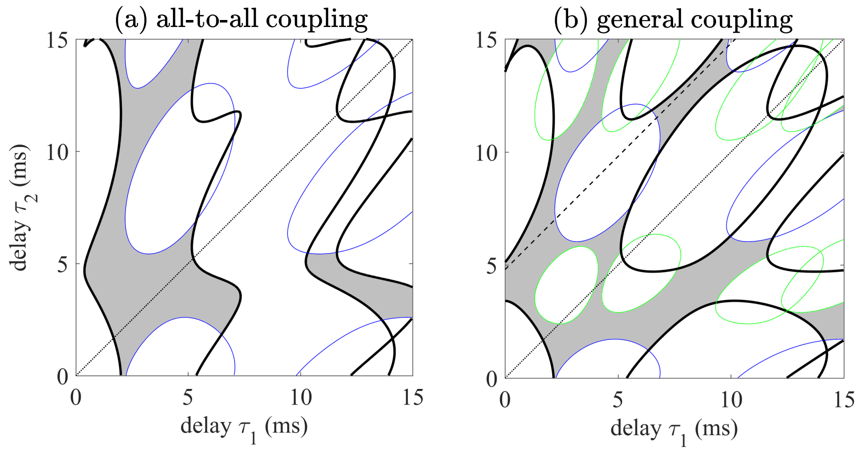

FIG. 3. Stability charts for the equilibrium of Hodgkin-Huxley neurons with (a) all-to-all coupling and (b) general coupling. Thick (black) curves are associated with purely imaginary roots of the tangential mode. Thin dark (blue) and light (green) curves indicate purely imaginary roots associated with mode 2 and 4/5, respectively. Stable regions, where all characteristic roots have negative real part, are shaded. The dotted and dashed lines in panel (b) correspond to Fig. 4(a) and (b), respectively.

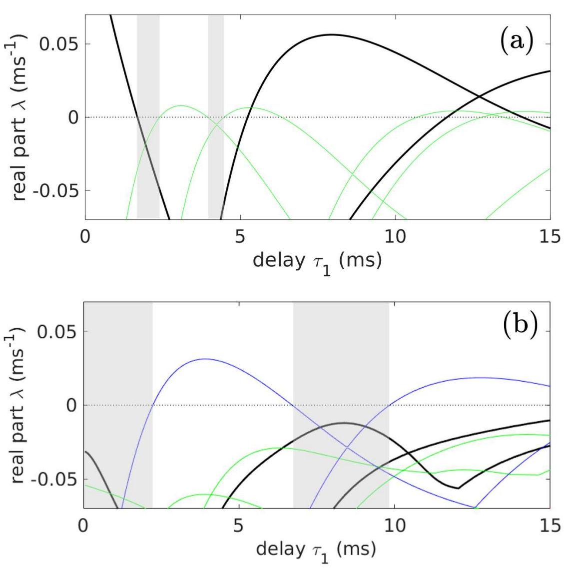

FIG. 4. Real part of characteristic roots for general coupling with (a) homogeneous delays $\tau_1 = \tau_2$ and (b) heterogeneous delays $\tau_2 = \tau_1 + 4.8$ ms (b); cf. Fig. 3(b). Stable regions are shaded. Color code as in Fig. 3 (only the dominant roots corresponding to modes 1,2 and 4/5 are shown).

B. Synchronous periodic spiking

The tools developed above allow us to study the stability of time-varying synchronized solutions. Here we study synchronized periodic solutions of the Hodgkin-Huxley neurons by analyzing the network dynamics within the synchronization manifold with the help of the software package DDE-BIFTOOL [56]. In other words, we compute periodic solutions of the n dimensional system Eq. (2) by using numerical collocation and continue these while varying the delays τ_1 and τ_2 with different values of the delay heterogeneity $\Delta\tau = \tau_2 - \tau_1$ as displayed in Fig. 5. Here the peak-to-peak voltage $|V_s|$, that is the difference between the maximum and the minimum voltage of the synchronized periodic solution, is used on the vertical axes. The left and the right columns in Fig. 5 correspond to the all-to-all (Eq. (25)) and the general coupling (Eq. (27)), respectively. DDE-BIFTOOL also provides us with the stability of the periodic solution with respect to perturbations within the synchronization manifold, where solid thin green (thick red) curves indicate tangentially stable (unstable) solutions. The stability with respect to transversal perturbations was calculated by decomposing the network dynamics as presented in Sec. III and analyzing the resulting periodic DDE with distributed delay Eq. (22) or Eq. (24) with the frequency domain method as described in Appendix A. The coefficient matrices $\mathbf{L}(t)$ and $\mathbf{R}(t)$ were calculated from the output of DDE-BIFTOOL and the operators $\mathcal{D}_k$ and $\mathcal{D}_{4,5}$ were taken from Sec. III D. While following each branch of periodic solutions, the dominant Floquet exponents associated with all $N-1$ transversal eigenmodes are calculated via Hill's infinite determinant Eq. (A10). Transversal instabilities are marked by dotted thick black curves in Fig. 5.

The solid thin (green) and solid thick (red) curves in Fig. 5(a) and (b) (for $\tau_1 = \tau_2$) are exactly the same because the tangential dynamics Eq. (7) are equivalent in case of homogeneous delays. However, due to different eigenvalues $\mathcal{D}_k$ of the adjacency lag operator for the all-to-all and the general coupling, we obtain different results for the stability with respect to transversal perturbations (dotted thick black curves). For example, for $\tau_1 = \tau_2 = 3.4$ ms both the synchronized equilib-

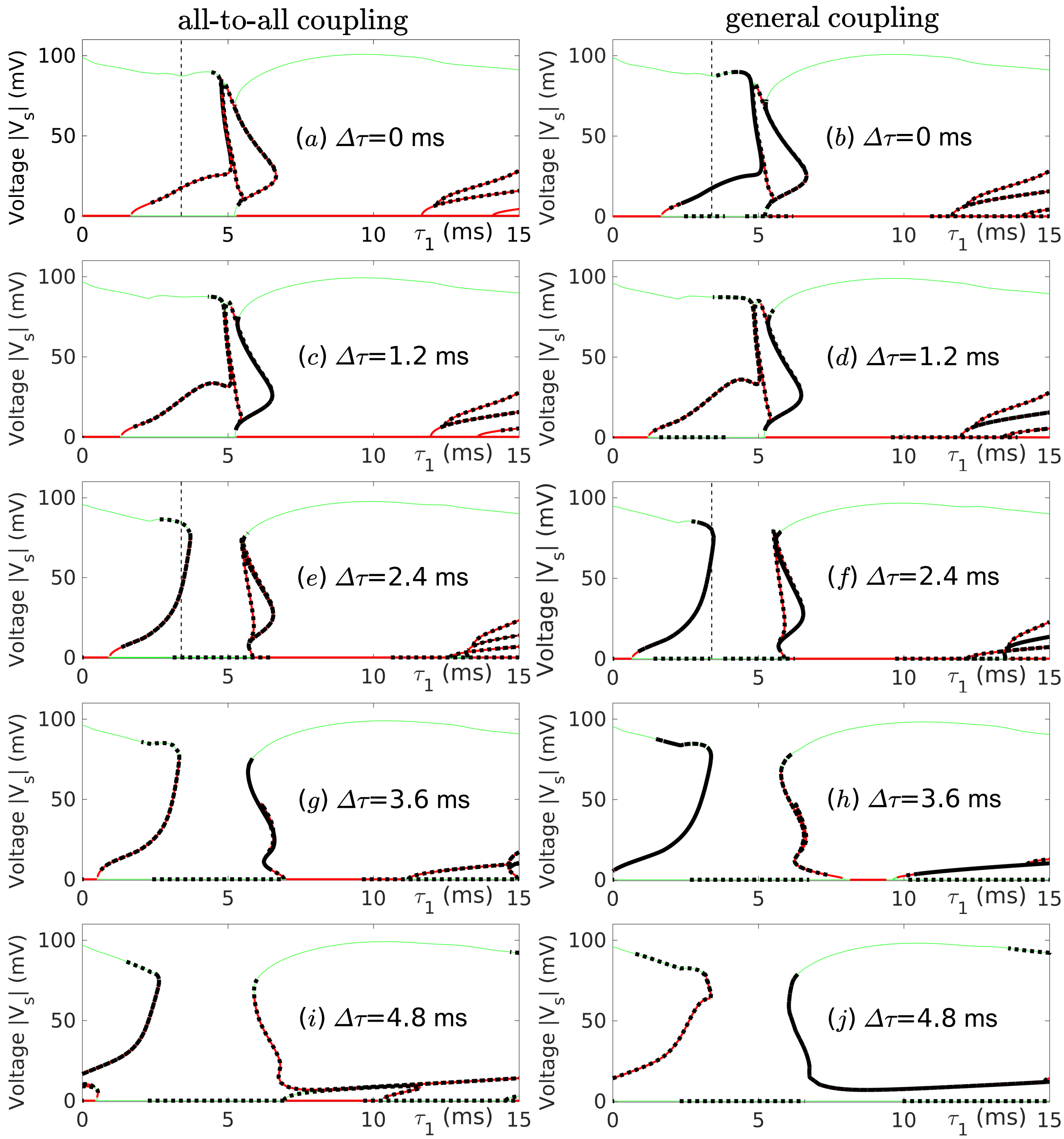

FIG. 5. Bifurcation diagrams for synchronized solutions of the Hodgkin-Huxley neurons for all-to-all coupling (left) and general coupling (right) and different values of the delay heterogeneity $\Delta\tau = \tau_2 - \tau_1$. The peak-to-peak voltage $|V_s|$ of the synchronized solutions for varying delay τ_1 are plotted. Solid thin green (thick red) curves represent stable (unstable) solutions with respect to tangential perturbations. Transversal instabilities are marked by dotted black curves. The dashed vertical lines in panels (a,b,e,f) are specific parameter sets that are used in Fig. 6. It can be seen that for increasing $\Delta\tau$ the parameter regions expand, where all synchronized periodic solutions are unstable or even no synchronized periodic solutions exist.

rium ($|V_s| = 0$ mV) and synchronized periodic spiking ($|V_s| \approx 90$ mV) is linearly stable for all-to-all coupling, whereas for general coupling the synchronized equilibrium is unstable; cf. solutions at the vertical dashed lines in Fig. 5(a) and (b), respectively. When increasing the delay heterogeneity $\Delta\tau = \tau_2 - \tau_1$, the parameter regions expand, where no synchronized periodic solutions exist. For example for $\Delta\tau = 4.8$ ms shown in Fig. 5(i) and (j) no such solutions exist for $\tau_1 \in [1.9, 5.9]$ ms and for $\tau_1 \in [1.4, 6.2]$ ms, respectively. In addition, the regions for transversal instabilities increase with increasing $\Delta\tau$, which further reduces the probability to observe synchronized periodic spiking. Moreover, transversal instabilities are more pronounced for the case of general cou-

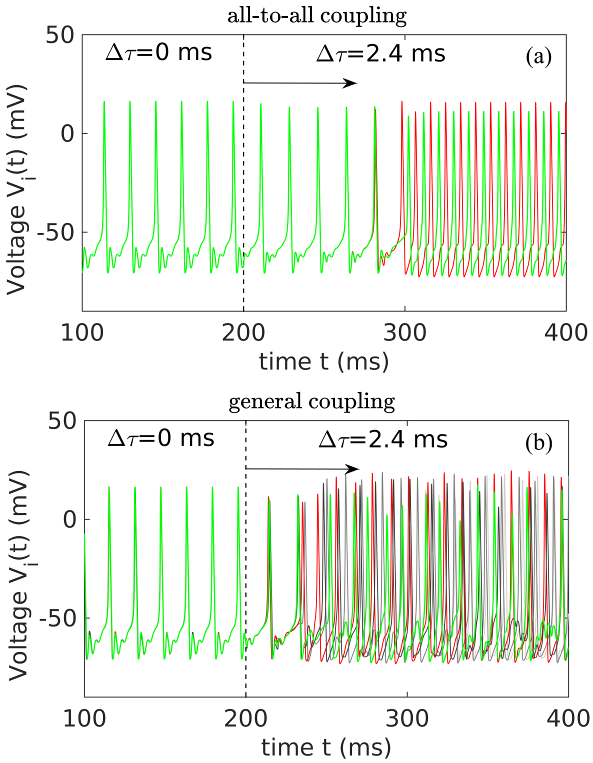

FIG. 6. Voltages of the Hodgkin-Huxley neurons Eq. (30) for all-to-all coupling (a) and general coupling (b). We set $\tau_1 = 3.4$ ms while heterogeneity in the delays is introduced at $t = 200$ ms by switching from $\Delta\tau = 0$ ms to $\Delta\tau = 2.4$ ms.

pling. For example, for all-to-all coupling with $\Delta\tau = 4.8$ shown in Fig. 5(i) synchronized periodic spiking is stable for $\tau_1 \in [0, 1.5]$ ms and $\tau_1 \in [6.0, 14.7]$ ms, whereas for the general coupling shown in Fig. 5(j) synchronized periodic spiking is only stable for $\tau_1 \in [0, 0.7]$ ms and $\tau_1 \in [6.4, 13.5]$ ms.

In order to demonstrate the full nonlinear dynamics of the Hodgkin-Huxley neurons we use numerical simulations. Specifically, Eq. (30) was integrated numerically with a Runge-Kutta method [57]. Arbitrary constant values are chosen for the initial functions. For $t < 200$ ms the delays were set to the homogeneous case $\tau_1 = \tau_2 = 3.4$ ms corresponding to the vertical dashed lines in Fig. 5(a) and (b). The voltages V_i of the five neurons are plotted as a function of time t for all-to-all coupling in Fig. 6(a) and for general coupling in Fig. 6(b). In both cases (after some transient dynamics not shown in Fig. 6) synchronized periodic spiking arose for $t < 200$ ms. At $t = 200$ ms, the delay τ_2 was increased abruptly to create the heterogeneity $\Delta\tau = \tau_2 - \tau_1 = 2.4$ ms corresponding to the vertical dashed lines in Fig. 5(e) and (f). Since in this case all possible synchronized solutions are transversally unstable, cluster-synchronized periodic spiking (for the all-to-all coupling) or asynchronous spiking (for the general coupling) appears.

V. CONCLUSION

Synchronized solutions of networks with heterogeneous coupling delays were investigated. The conditions for the existence of the synchronization manifold were given. It was shown that adding heterogeneity in the delays may destroy time dependent synchronized solutions while still maintain synchronized equilibria.

A systematic method was presented for the decomposition of the dynamics at the network level in the vicinity of synchronized solutions. This was based on the decomposition of the adjacency lag operator, which contains information about the network topology as well as the coupling delays. Conditions were given for the modes to be decoupled. In the generic case, a diagonalization of the adjacency lag operator leads only to a triangular structure for the network dynamics. This is a fundamental difference to synchronized equilibria, where a diagonalization of the adjacency lag operator decouples the network dynamics [5]. Due to the triangular structure, indeed, for time dependent synchronized solutions the stability of the complete network dynamics can be analyzed by several lower dimensional blocks in the main diagonal, but the unstable directions cannot be identified uniquely. The low dimensional blocks that determine the stability of the network modes are DDEs with distributed delay, where the stability of different modes is associated with different delay distributions.

As an example, the effects of delay heterogeneity on synchronized equilibria and synchronized periodic spiking in a systems of Hodgkin-Huxley neurons were studied. It turns out that increasing the heterogeneity in the coupling delays leads to larger regions where all synchronized periodic solutions are unstable or even no synchronized periodic solutions exist. As neurosystems often store information using periodic cluster-synchronized states, establishing mathematical tool for their stability analysis in the presence of heterogeneous delays is an interesting future research direction. The extension of the current work to near synchronous states is another interesting direction for future research.

ACKNOWLEDGMENTS

D.B. acknowledges support from the Hungarian Scientific Research Fund - OTKA PD-112983 and the Janos Bolyai Research Scholarship of the Hungarian Academy of Sciences.

[1] X. Li, Y. Y. Jin, and G. Chen, Physica A **328**, 287 (2003).

[2] A. Pluchino, V. Latora, and A. Rapisarda, Int. J. Mod. Phys. C **16**, 515 (2005).

[3] M. Rohden, A. Sorge, M. Timme, and D. Witthaut, Phys. Rev. Lett. **109**, 064101 (2012).
[4] F. M. Atay, Phil. Trans. Royal Soc. A **371** (2013).
[5] R. Szalai and G. Orosz, Phys. Rev. E **88**, 040902 (2013).
[6] K. Schmietendorf, J. Peinke, R. Friedrich, and O. Kamps, Eur. Phys. J. Spec. Top. **223**, 2577–2592 (2014).
[7] L. Glass, Nature **410**, 277 (2001).
[8] E. Rossoni, Y. Chen, M. Ding, and J. Feng, Phys. Rev. E **71**, 061904 (2005).
[9] E. Schöll, G. Hiller, P. Hövel, and M. A. Dahlem, Phil. Trans. Royal Soc. A **367**, 1079 (2009).
[10] G. Orosz, in *Delay Systems*, Advances in Delays and Dynamics, Vol. 1, edited by T. Vyhlídal, J.-F. Lafay, and R. Sipahi (Springer, 2014) pp. 343–357.
[11] S. Zhu, X. Chen, X. Lu, K. S. Thornburg Jr., G. D. Vanwiggeren, and R. Roy, in *Frontiers of Laser Physics and Quantum Optics*, edited by Z. Xu, S. Xie, S.-Y. Zhu, and M. Scully (Springer, 2000) pp. 631–634.
[12] T. Heil, I. Fischer, W. Elsässer, J. Mulet, and C. R. Mirasso, Phys. Rev. Lett. **86**, 795 (2001).
[13] V. Flunkert and E. Schöll, New J. Phys. **14**, 033039 (2012).
[14] A. Pikovsky, M. Rosenblum, and J. Kurths, *Synchronization: A Universal Concept in Nonlinear Sciences* (Cambridge University Press, 2003).
[15] A. Arenas, A. Díaz-Guilera, J. Kurths, Y. Moreno, and C. Zhou, Phys. Rep. **469**, 93 (2008).
[16] F. M. Atay, J. Jost, and A. Wende, Phys. Rev. Lett. **92**, 144101 (2004).
[17] V. Flunkert, S. Yanchuk, T. Dahms, and E. Schöll, Phys. Rev. Lett. **105**, 254101 (2010).
[18] M. Lakshmanan and D. V. Senthilkumar, *Dynamics of Nonlinear Time-Delay Systems* (Springer, 2011).
[19] F. M. Atay, Phys. Rev. Lett. **91**, 094101 (2003).
[20] C. Masoller and A. Mart'ı, Phys. Rev. Lett. **94**, 134102 (2005).
[21] A. Panchuk, D. P. Rosin, P. Hövel, and E. Schöll, Int. J. Bifur. Chaos **23**, 1330039 (2013).
[22] C. Cakan, J. Lehnert, and E. Schöll, Eur. Phys. J. B **87**, 54 (2014).
[23] L. M. Pecora and T. Carroll, Phys. Rev. Lett. **80**, 2109 (1998).
[24] L. M. Pecora, Phys. Rev. E **58**, 347 (1998).
[25] J. Sun, E. M. Bollt, and T. Nishikawa, EPL **85**, 60011 (2009).
[26] F. Sorrentino and M. Porfiri, EPL **93**, 50002 (2011).
[27] T. Dahms, J. Lehnert, and E. Schöll, Phys. Rev. E **86**, 016202 (2012).
[28] G. Orosz, SIAM J. Appl. Dyn. Sys. **13**, 1353 (2014).
[29] L. M. Pecora, F. Sorrentino, A. M. Hagerstrom, T. E. Murphy, and R. Roy, Nat. Commun **5**, 4079 (2014).
[30] A. Englert, W. Kinzel, Y. Aviad, M. Butkovski, I. Reidler, M. Zigzag, I. Kanter, and M. Rosenbluh, Phys. Rev. Lett. **104**, 114102 (2010).
[31] K. Konishi, H. Kokame, and N. Hara, Phys. Rev. E **81**, 016201 (2010).
[32] M. Zigzag, M. Butkovski, A. Englert, W. Kinzel, and I. Kanter, Phys. Rev. E **81**, 036215 (2010).
[33] A. Gjurchinovski, A. Zakharova, and E. Schöll, Phys. Rev. E **89**, 032915 (2014).
[34] A. Englert, S. Heiligenthal, W. Kinzel, and I. Kanter, Phys. Rev. E **83**, 046222 (2011).
[35] O. D'Huys, S. Zeeb, T. Jüngling, S. Heiligenthal, S. Yanchuk, and W. Kinzel, EPL **103**, 10013 (2013).
[36] A. Otto and G. Radons, Proc. 9th Int. Conf. on HSM, San Sebastian, Spain (2012).
[37] D. Bachrathy and G. Stépán, CIRP Annals **62**, 411 (2013).
[38] We call the time-invariant homogeneous state of the network synchronized equilibria even if it does not fulfill the definition of synchronization according to Ref. [14].
[39] S. Gurevich and R. Friedrich, Phys. Rev. Lett. **110**, 014101 (2013).
[40] S. Gurevich, Phys. Rev. E **87**, 052922 (2013).
[41] P. C. Matthews and S. H. Strogatz, Phys. Rev. Lett. **65**, 1701 (1990).
[42] D. V. Ramana Reddy, A. Sen, and G. L. Johnston, Phys. Rev. Lett. **85**, 3381 (2000).
[43] V. Resmi, G. Ambika, and R. E. Amritkar, Phys. Rev. E **84**, 046212 (2011).
[44] G. Stépán, *Retarded Dynamical Systems: Stability and Characteristic Functions* (Longman Scientific & Technical, 1989).
[45] J. K. Hale and S. M. Verduyn Lunel, *Introduction to Functional Differential Equations*, Appl. Math. Sci. No. 99 (Springer, 1993).
[46] C. Hwang and Y.-C. Cheng, Automatica **41**, 1979 (2005).
[47] E. Jarlebring and T. Damm, Automatica **43**, 2124 (2007).
[48] R. Bellmann and K. L. Cooke, *Differential-Difference Equations* (Academic Press, 1963).
[49] A. Amann, E. Schöll, and W. Just, Physica A: Stat. Mech. Appl. **373**, 191 (2007).
[50] S. Yi, P. W. Nelson, and A. G. Ulsoy, *Time Delay Systems: Analysis and Control Using the Lambert W Function* (World Scientific, 2010).
[51] A. L. Hodgkin and A. F. Huxley, Journal of Physiology **117**, 500 (1952).
[52] A. Otto, *Frequency domain methods for the analysis of time delay systems*, Ph.D. thesis, TU Chemnitz (2016).
[53] Z. Dombovari, Y. Altintas, and G. Stépán, Int. J. Mach. Tools Manuf. **50**, 511 (2010).
[54] Z. Dombovari and G. Stepan, ASME. J. Manuf. Sci. Eng. **134**, 051015 (2012).
[55] A. Otto, S. Rauh, S. Ihlenfeldt, and G. Radons, Int. J. Adv. Manuf. Technol. **89**, 2613 (2017).
[56] J. Sieber, K. Engelborghs, T. Luzyanina, G. Samaey, and D. Roose, (2014), arXiv:1406.7144 [math.DS].
[57] L. F. Shampine, Appl. Num. Math. **52**, 113 (2005).
[58] W. Michiels and S.-I. Niculescu, *Stability and Stabilization of Time-Delay Systems* (SIAM, 2007).
[59] D. Bachrathy and G. Stépán, Period. Polytech., Mech. Eng. **56**, 81 (2012).
[60] G. W. Hill, Acta Math. **8**, 1 (1886).
[61] B. P. Lampe, E. N. Rosenwasser, and L. Berg, in *16th Int. Conf. MMAR, Miedzyzdroje, Poland* (2011) pp. 100–106.
[62] Y. Altintas, G. Stépán, D. Merdol, and Z. Dombovári, CIRP J. Manuf. Sci. Technol. **1**, 35 (2008).
[63] Y. Altintas, *Manufacturing Automation: Metal Cutting Mechanics, Machine Tool Vibrations, and CNC Design* (Cambridge University Press, 2012).
[64] T. Insperger and G. Stépán, R. Soc. Lond. Proc. Ser. A Math. Phys. Eng. Sci. **458**, 1989 (2002).
[65] M. Farkas, *Periodic Motions* (Springer, 1994).

Appendix A: Stability analysis in the frequency domain

A frequency domain approach is suitable for the stability analysis of the modal dynamics Eq. (22) and Eq. (24) because exponential functions e^{st} are eigenfunctions of the lag operator (cf. Eq. (12)). For synchronized equilibria $\boldsymbol{x}_\mathrm{s}(t) \equiv \boldsymbol{x}_\mathrm{s}^*$, Eq. (22) with time invariant coefficient matrices $\mathbf{L}(t) = \mathbf{L}_0$ and $\mathbf{R}(t) = \mathbf{R}_0$ can be used for the description of the modal dynamics. Then, the exponential ansatz

$$\boldsymbol{q}_k(t) = \hat{\boldsymbol{q}}_{k,0}\,\mathrm{e}^{st} \tag{A1}$$

with $s \in \mathbb{C}$ can be substituted into Eq. (22) (see [44, 48, 49, 58]), which leads to the modal characteristic equation

$$\det\left[\mathbf{I}_n s - \mathbf{L}_0 - \mathbf{R}_0 \Lambda_k(s)\right] = 0, \tag{A2}$$

where $\Lambda_k(s)$ is the frequency domain representation of $\mathcal{D}_k$. In fact, we can define $\Lambda_k(s)$ as the eigenvalue of the operator $\mathcal{D}_k$, i.e.,

$$\mathcal{D}_k\,\mathrm{e}^{st} = \Lambda_k(s)\,\mathrm{e}^{st}\,. \tag{A3}$$

Recall that $\mathrm{e}^{-s\tau}$ is the eigenvalue of the lag operator $\mathcal{S}(\tau)$; see Eq. (12). For example, when $\mathcal{D}_k$ can be written in the form Eq. (21), we have

$$\Lambda_k(s) = \sum_{r=1}^{R} \sigma_{r,k}\;\mathrm{e}^{-s\tau_r}\,. \tag{A4}$$

The discrete spectrum of the DDE, i.e., the characteristic roots s, can be found by solving the characteristic equation Eq. A2. The characteristic roots determine the stability of the kth network mode: if all characteristic roots are located in the left-half of the complex plane then the mode is stable. Although there are infinitely many characteristic roots, those with the largest real part, often called dominant roots, determine the stability. In this paper we compute these roots by using a multi-dimensional bisection method [37, 59]. As the parameters (e.g., the delays) are varied, roots can move into the right-half of the complex plane resulting in an instability. The stability boundaries indicate the parameter values where roots cross the imaginary axis. By substituting $s = i\omega$, $\omega \geq 0$ into Eq. A2 one may find these boundaries explicitly.

The frequency domain stability analysis for synchronized periodic solutions $\boldsymbol{x}_\mathrm{s}(t) = \boldsymbol{x}_\mathrm{s}(t+T)$, where T denotes the period, is based on Hill's infinite determinant method [60, 61]. The method is often used in engineering applications and it is also known as multifrequency approach [36, 37, 62–64]. Here we present the formula only for the analysis of Eq. (22) but the approach can be easily extended to the analysis of Eq. (24). For synchronized periodic solutions the coefficient matrices are periodic, that is, $\mathbf{L}(t) = \mathbf{L}(t+T)$ and $\mathbf{R}(t) = \mathbf{R}(t+T)$. From Floquet theory it is known that the solutions Eq. (22) can be written as

$$\boldsymbol{q}_k(t) = \boldsymbol{p}_k(t)\,\mathrm{e}^{st}, \quad \boldsymbol{p}_k(t) = \boldsymbol{p}_k(t+T), \tag{A5}$$

where the complex numbers $s \in \mathbb{C}$ are called Floquet exponents; see [65]. The periodic part $\boldsymbol{p}_k(t)$ can be expanded using Fourier series

$$\boldsymbol{p}_k(t) = \sum_{l=-\infty}^{\infty} \hat{\boldsymbol{q}}_{k,l}\,\mathrm{e}^{\mathrm{i}l\Omega t} \;\;\Rightarrow\;\; \boldsymbol{q}_k(t) = \sum_{l=-\infty}^{\infty} \hat{\boldsymbol{q}}_{k,l}\,\mathrm{e}^{(s+\mathrm{i}l\Omega)t}, \tag{A6}$$

where i is the imaginary unit, $\Omega = 2\pi/T$ is the frequency and $\hat{\boldsymbol{q}}_{k,l}$ are the Fourier coefficients. Similarly, the periodic matrices $\mathbf{L}(t)$ and $\mathbf{R}(t)$ can be expanded into Fourier series

$$\mathbf{L}(t) = \sum_{m=-\infty}^{\infty} \mathbf{L}_m\,\mathrm{e}^{\mathrm{i}m\Omega t}, \quad \mathbf{R}(t) = \sum_{m=-\infty}^{\infty} \mathbf{R}_m\,\mathrm{e}^{\mathrm{i}m\Omega t}\,. \tag{A7}$$

Putting Eq. (A6) and Eq. (A7) into the modal dynamics Eq. (22) yields

$$\sum_{m=-\infty}^{\infty} \mathrm{e}^{\mathrm{i}m\Omega t} \sum_{l=-\infty}^{\infty} \mathbf{M}_{m,l}\,\hat{\boldsymbol{q}}_{k,l} = 0, \tag{A8}$$

where the matrices $\mathbf{M}_{m,l}$ are given by

$$\mathbf{M}_{m,l} = \mathbf{I}_n(s+\mathrm{i}l\Omega)\,\delta_{m,l} - \mathbf{L}_{m-l} - \mathbf{R}_{m-l}\,\Lambda_k(s+\mathrm{i}l\Omega). \tag{A9}$$

and $\Lambda_k(s)$ are defined in Eq. (A3). Since in Eq. (A8) the coefficients for each harmonic m must vanish, we obtain

$$\det\begin{bmatrix} \ddots & & \vdots & & \iddots \\ & \mathbf{M}_{-1,-1} & \mathbf{M}_{-1,0} & \mathbf{M}_{-1,1} & \\ \cdots & \mathbf{M}_{0,-1} & \mathbf{M}_{0,0} & \mathbf{M}_{0,1} & \cdots \\ & \mathbf{M}_{1,-1} & \mathbf{M}_{1,0} & \mathbf{M}_{1,1} & \\ \iddots & & \vdots & & \ddots \end{bmatrix} = 0. \tag{A10}$$

which is an infinite determinant and can be interpreted as the characteristic equation of the DDE Eq. (22) for periodic coefficient matrices. Note that the matrices $\mathbf{M}_{m,l}$ also depend on the modal index k.

If the coefficient matrices $\mathbf{L}(t), \mathbf{R}(t)$ are constant, the higher harmonics in Eq. (A7) vanish, i.e., $\mathbf{L}_m = \mathbf{R}_m = \mathbf{0}$ for $m \neq 0$, and Eq. (A10) simplify to Eq. (A2). In general, the Fourier coefficients $\mathbf{L}_m$ and $\mathbf{R}_m$ depend on the form of the synchronized periodic solution of the network, which is often available only numerically. Again, stability is guaranteed when all Floquet exponents s are located in the left-half of the complex plane. We use the multi-dimensional bisection method to compute the exponents and detect the stability boundaries in parameter space [37, 59] but one may find alternative methods in [52]. For a practical calculation of the determinant Eq. (A10), the infinite matrix $\mathbf{M}$ is truncated to a finite dimensional matrix by taking into account only a finite number of higher harmonics [36, 37, 62, 63]. Finally, we remark that ansatzes similar to Eq. (A1) or Eq. (A5) can also be made in the original system Eq. (6) leading to a complete frequency domain description of the network dynamics.

Appendix B: Network modes for the examples

For simplicity we introduce the notation $\mathcal{S}(\tau_1) = \mathcal{S}_1$, $\mathcal{S}(\tau_2) = \mathcal{S}_2$. The operator-valued left and right eigenvectors for the all-to-all coupling corresponding to the operator-valued eigenvalues of Eq. (26) are given by

$$\mathcal{V}_1 = \begin{bmatrix} 1 \\ 1 \\ 1 \\ 1 \\ 1 \end{bmatrix}, \quad \mathcal{V}_2 = \begin{bmatrix} 1 \\ -\frac{3}{2} \\ -\frac{3}{2} \\ 1 \\ 1 \end{bmatrix}, \quad \mathcal{V}_3 = \frac{1}{4\mathcal{S}_1 + \mathcal{S}_2} \begin{bmatrix} \mathcal{S}_1 \\ \mathcal{S}_1 \\ \mathcal{S}_1 \\ -(3\mathcal{S}_1 + \mathcal{S}_2) \\ \mathcal{S}_1 \end{bmatrix}, \quad \mathcal{V}_4 = \begin{bmatrix} 0 \\ \frac{1}{2} \\ -\frac{1}{2} \\ 0 \\ 0 \end{bmatrix}, \quad \mathcal{V}_5 = \frac{1}{3\mathcal{S}_1 + 2\mathcal{S}_2} \begin{bmatrix} \mathcal{S}_1 + \mathcal{S}_2 \\ -\frac{1}{2}\mathcal{S}_1 \\ -\frac{1}{2}\mathcal{S}_1 \\ \mathcal{S}_1 + \mathcal{S}_2 \\ -(2\mathcal{S}_1 + \mathcal{S}_2) \end{bmatrix}, \tag{B1}$$

and

$$\begin{aligned} \mathcal{U}_1 &= \begin{bmatrix} \frac{1}{5}\frac{13\mathcal{S}_1^2+9\mathcal{S}_1\mathcal{S}_2+3\mathcal{S}_2^2}{(4\mathcal{S}_1+\mathcal{S}_2)(3\mathcal{S}_1+2\mathcal{S}_2)} & \frac{1}{5} & \frac{1}{5} & \frac{\mathcal{S}_1}{4\mathcal{S}_1+\mathcal{S}_2} & \frac{1}{5}\frac{2\mathcal{S}_1+3\mathcal{S}_2}{3\mathcal{S}_1+2\mathcal{S}_2} \end{bmatrix}, \\ \mathcal{U}_2 &= \begin{bmatrix} \frac{1}{5} & -\frac{1}{5} & -\frac{1}{5} & 0 & \frac{1}{5} \end{bmatrix}, \\ \mathcal{U}_3 &= \begin{bmatrix} 1 & 0 & 0 & -1 & 0 \end{bmatrix}, \\ \mathcal{U}_4 &= \begin{bmatrix} 0 & 1 & -1 & 0 & 0 \end{bmatrix}, \\ \mathcal{U}_5 &= \begin{bmatrix} 1 & 0 & 0 & 0 & -1 \end{bmatrix}. \end{aligned} \tag{B2}$$

The operator-valued left and right eigenvectors corresponding to the general coupling with $\mathcal{D}_1$, $\mathcal{D}_2$ and $\mathcal{D}_3$ from Eq. (28) corresponding to the master and slave modes and $\mathcal{D}_{4,5}$ from Eq. (29) corresponding to the intermediate modes are given by

$$\begin{aligned} &\mathcal{V}_1 = \begin{bmatrix} 1 \\ 1 \\ 1 \\ 1 \\ 1 \end{bmatrix}, \quad \mathcal{V}_2 = \begin{bmatrix} 1 \\ -2 \\ -2 \\ 1 \\ 1 \end{bmatrix}, \quad \mathcal{V}_3 = \frac{1}{2}\frac{1}{(\mathcal{S}_1 + \mathcal{S}_2)(\mathcal{S}_1 - 2\mathcal{S}_2)} \begin{bmatrix} \mathcal{S}_1^2 - 2\mathcal{S}_2^2 \\ -\mathcal{S}_1^2 \\ -\mathcal{S}_1^2 \\ \mathcal{S}_1^2 - 2\mathcal{S}_2^2 \\ -(\mathcal{S}_1^2 - 2\mathcal{S}_1\mathcal{S}_2 - 2\mathcal{S}_2^2) \end{bmatrix}, \\ &\mathcal{V}_{4,5} = \frac{1}{(\mathcal{S}_1^2 - \mathcal{S}_1\mathcal{S}_2 + 2\mathcal{S}_2^2)(7\mathcal{S}_1^2 + 8\mathcal{S}_1\mathcal{S}_2 + 2\mathcal{S}_2^2)} \\ &\quad\times \begin{bmatrix} \mathcal{S}_1(\mathcal{S}_1^3 - \mathcal{S}_1\mathcal{S}_2^2 - \mathcal{S}_2^3) & \mathcal{S}_1(2\mathcal{S}_1^3 + 2\mathcal{S}_1^2\mathcal{S}_2 + 5\mathcal{S}_1\mathcal{S}_2^2 + 4\mathcal{S}_2^3) \\ \mathcal{S}_1^4 + 6\mathcal{S}_1^2\mathcal{S}_2^2 + 7\mathcal{S}_1\mathcal{S}_2^3 + 2\mathcal{S}_2^4 & \mathcal{S}_1(2\mathcal{S}_1^3 - 5\mathcal{S}_1^2\mathcal{S}_2 - 3\mathcal{S}_1\mathcal{S}_2^2 + 2\mathcal{S}_2^3) \\ -6\mathcal{S}_1^4 - \mathcal{S}_1^3\mathcal{S}_2 - 2\mathcal{S}_1^2\mathcal{S}_2^2 - 7\mathcal{S}_1\mathcal{S}_2^3 - 2\mathcal{S}_2^4 & \mathcal{S}_1(2\mathcal{S}_1^3 - 5\mathcal{S}_1^2\mathcal{S}_2 - 3\mathcal{S}_1\mathcal{S}_2^2 + 2\mathcal{S}_2^3) \\ \mathcal{S}_1(\mathcal{S}_1^3 - \mathcal{S}_1\mathcal{S}_2^2 - \mathcal{S}_2^3) & -5\mathcal{S}_1^4 + \mathcal{S}_1^3\mathcal{S}_2 - 3\mathcal{S}_1^2\mathcal{S}_2^2 - 10\mathcal{S}_1\mathcal{S}_2^3 - 4\mathcal{S}_2^4 \\ \mathcal{S}_1(\mathcal{S}_1^3 - \mathcal{S}_1\mathcal{S}_2^2 - \mathcal{S}_2^3) & \mathcal{S}_1(2\mathcal{S}_1^3 + 2\mathcal{S}_1^2\mathcal{S}_2 + 5\mathcal{S}_1\mathcal{S}_2^2 + 4\mathcal{S}_2^3) \end{bmatrix}, \end{aligned} \tag{B3}$$

and

$$\begin{aligned} \mathcal{U}_1 &= \begin{bmatrix} \frac{1}{6}\frac{9\mathcal{S}_1^3+16\mathcal{S}_1^2\mathcal{S}_2+12\mathcal{S}_1\mathcal{S}_2^2+4\mathcal{S}_2^3}{(\mathcal{S}_1+\mathcal{S}_2)(7\mathcal{S}_1^2+8\mathcal{S}_1\mathcal{S}_2+2\mathcal{S}_2^2)} & \frac{(\mathcal{S}_1+\mathcal{S}_2)(4\mathcal{S}_1+\mathcal{S}_2)}{21\mathcal{S}_1^2+24\mathcal{S}_1\mathcal{S}_2+6\mathcal{S}_2^2} & \frac{3\mathcal{S}_1^2+3\mathcal{S}_1\mathcal{S}_2+\mathcal{S}_2^2}{21\mathcal{S}_1^2+24\mathcal{S}_1\mathcal{S}_2+6\mathcal{S}_2^2} & \frac{\mathcal{S}_1(6\mathcal{S}_1+5\mathcal{S}_2)}{21\mathcal{S}_1^2+24\mathcal{S}_1\mathcal{S}_2+6\mathcal{S}_2^2} & \frac{1}{6}\frac{\mathcal{S}_1+2\mathcal{S}_2}{\mathcal{S}_1+\mathcal{S}_2} \end{bmatrix}, \\ \mathcal{U}_2 &= \begin{bmatrix} -\frac{1}{3}\frac{\mathcal{S}_2(2\mathcal{S}_1^2-3\mathcal{S}_1\mathcal{S}_2+2\mathcal{S}_2^2)}{(\mathcal{S}_1-2\mathcal{S}_2)(\mathcal{S}_1^2-\mathcal{S}_1\mathcal{S}_2+2\mathcal{S}_2^2)} & -\frac{1}{3}\frac{\mathcal{S}_1^2-\mathcal{S}_1\mathcal{S}_2+\mathcal{S}_2^2}{\mathcal{S}_1^2-\mathcal{S}_1\mathcal{S}_2+2\mathcal{S}_2^2} & -\frac{1}{3}\frac{\mathcal{S}_2^2}{\mathcal{S}_1^2-\mathcal{S}_1\mathcal{S}_2+2\mathcal{S}_2^2} & \frac{1}{3}\frac{\mathcal{S}_1\mathcal{S}_2}{\mathcal{S}_1^2-\mathcal{S}_1\mathcal{S}_2+2\mathcal{S}_2^2} & \frac{1}{3}\frac{\mathcal{S}_1-\mathcal{S}_2}{\mathcal{S}_1-2\mathcal{S}_2} \end{bmatrix}, \\ \mathcal{U}_3 &= \begin{bmatrix} 1 & 0 & 0 & 0 & -1 \end{bmatrix}, \\ \mathcal{U}_{4,5} &= \begin{bmatrix} 0 & 1 & -1 & 0 & 0 \\ 1 & 0 & 0 & -1 & 0 \end{bmatrix}. \end{aligned} \tag{B4}$$

Appendix C: Details of the Hodgkin-Huxley model

The nonlinear functions used in the the Hodgkin-Huxley model Eq. (30) are

$$\begin{aligned} \alpha_m(V) &= \frac{0.1\,(V+40)}{1-\mathrm{e}^{-\frac{V+40}{10}}}, \quad \beta_m(V) = 4\,\mathrm{e}^{-\frac{V+65}{18}}, \\ \alpha_h(V) &= 0.07\,\mathrm{e}^{-\frac{V+65}{20}}, \quad \beta_h(V) = \frac{1}{1+\mathrm{e}^{-\frac{V+35}{10}}}, \\ \alpha_n(V) &= \frac{0.01\,(V+55)}{1-\mathrm{e}^{-\frac{V+55}{10}}}, \quad \beta_n(V) = 0.125\,\mathrm{e}^{-\frac{V+65}{80}}. \end{aligned} \tag{C1}$$

while the parameters used in Eq. (30) are given in Table I.

TABLE I. Parameters for Hodgkin-Huxley neurons.

$V_{\mathrm{Na}} = 50$ mV	$g_{\mathrm{Na}} = 120\,\frac{\mathrm{mS}}{\mathrm{cm}^2}$	$C = 1\,\frac{\mu\mathrm{F}}{\mathrm{cm}^2}$
$V_{\mathrm{K}} = -77$ mV	$g_{\mathrm{K}} = 36\,\frac{\mathrm{mS}}{\mathrm{cm}^2}$	$I = 20\,\frac{\mu\mathrm{A}}{\mathrm{cm}^2}$
$V_{\mathrm{L}} = -54.4$ mV	$g_{\mathrm{L}} = 0.3\,\frac{\mathrm{mS}}{\mathrm{cm}^2}$	$N = 5$